Clouds and the Earth's Radiant Energy System (CERES)

Algorithm Theoretical Basis Document

Convolution of Imager Cloud Properties With CERES Footprint Point Spread Function (Subsystem 4.4)

Richard Green[1]
Bruce A. Wielicki[1]

[1]Atmospheric Sciences Division, NASA Langley Research Center, Hampton, Virginia 23681-0001

June 2, 1997

CERES Top Level Data Flow Diagram

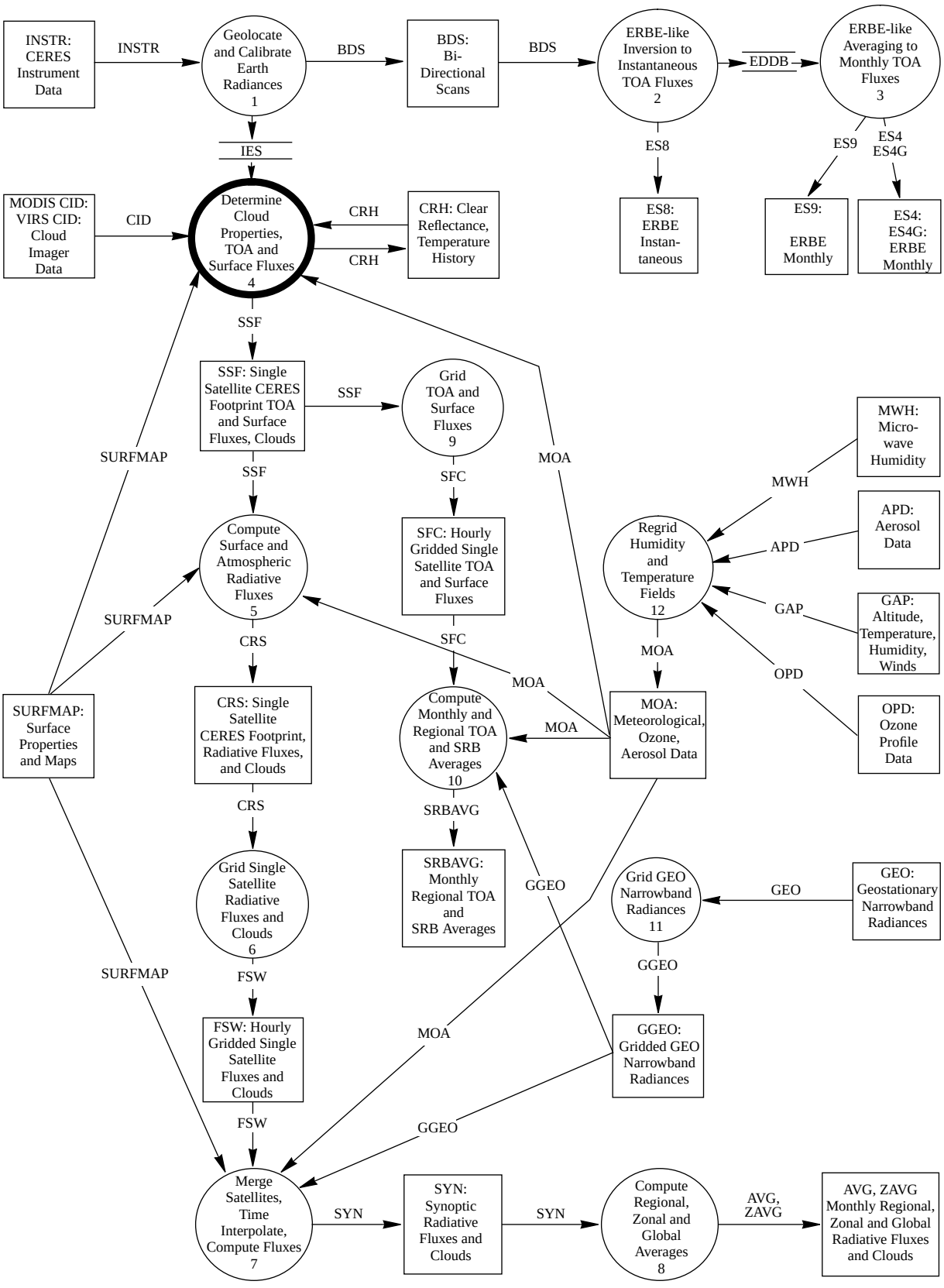

Abstract

CERES will determine the Earth Radiation Budget (ERB) at the top-of-the-atmosphere (TOA) and at the surface of the Earth. To determine the surface ERB we must know the cloud properties over the CERES footprint. We use imager data at high resolution to get the necessary cloud properties. First, we locate the imager pixels that are within the CERES footprint. Since CERES has a rotating azimuth plane scanner, the collocation algorithm must be capable of handling an elongated and skewed footprint. We then determine the cloud statistics over the footprint with the cloud properties from the high resolution imager cloud properties. Our statistics are weighted means and standard deviations where the weighting is the value of the point spread function (PSF). The major input and output data are defined in Appendices A and B of section 4.0.

4.4.1 INTRODUCTION

The general process is to analyze a large swath (approximately 500 km) of imager data as a unit and define cloud properties at each imager observation point (approximately 2 km grid). This requires multiple auxiliary data and various algorithms working in conjunction with one another. Once the 500 km swath of imager data is analyzed, the cloud statistics are determined over the CERES footprint. This footprint is defined by the CERES point spread function which gives the appropriate weighting of the field with respect to the optical axis. In other words, we form a CERES “cookie cutter” and cut out the cloud properties from the larger and higher resolution imager swath. This process continues with successive CERES footprints organized spatially along the satellite groundtrack until we are within 100 km of the end of the 500-km swath. If we proceed beyond this point part of the CERES footprint could fall beyond the 500-km swath. At this point we drop the last 300 km of imager data, retain 200 km of data in the current area of convolution, and add a new 300 km swath at the beginning. Thus, we have a new 500-km swath and continue as before.

4.4.2 ALGORITHM DESCRIPTION

4.4.2.1. CERES Point Spread Function

The CERES scanning radiometer is an evolutionary development of the ERBE scanning radiometer. It is desired to increase the resolution as much as possible, using a thermistor bolometer as the detector. As the resolution is increased, the sampling rate must increase to achieve the desired resolution. When the sampling rate becomes comparable to the response time of the detector, the effect of the time response of the detector on the point spread function (PSF) must be considered. Also, the signal is usually filtered electronically prior to sampling in order to attenuate electronic noises and to remove high frequency components of the signal which would cause aliasing errors. The time response of the filter together with that of the detector will cause a lag in the output relative to the input radiance, so that the time response causes the centroid of the PSF to be displaced from the centroid of the optical field-of-view. Thus, the signal as sampled is coming not only from where the radiometer is pointed, but includes a “memory” of the input from where it had been looking. Another effect of the time response is to broaden the PSF, which will reduce the resolution of the measurement, increase blurring errors, and decrease aliasing errors.

A full discussion of the point spread function and its development are given in Smith (1994) and a graph of the function is given in Figure 1-5. We will only define the function here. From Figure 4.4-2 we redraw half of the optical FOV in Figure 4.4-1 where δ' is the along-scan angle

$$\delta'_f(\beta) = \begin{cases} -a & 0 \le \beta < a \\ -2a + \beta & a \le \beta < 2a \end{cases}$$

$$\delta'_b(\beta) = \begin{cases} a & 0 \le \beta < a \\ 2a - \beta & a \le \beta < 2a \end{cases}$$

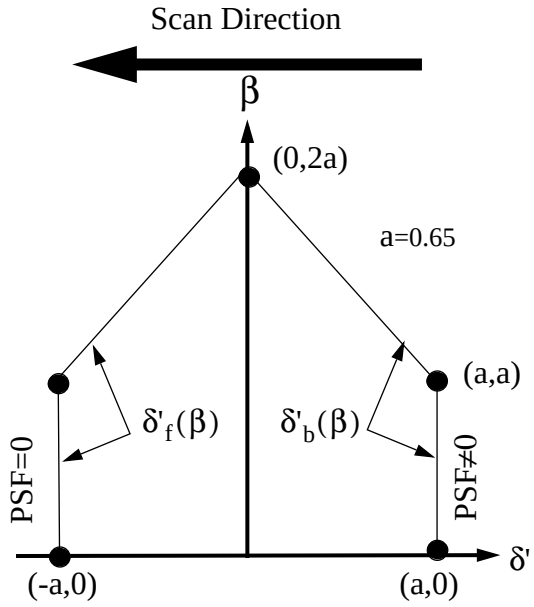

Figure 4.4-1. Optical FOV

and β is the cross-scan angle. Note that δ' points opposite the scan direction and increases toward the tail of the PSF (see Figure 4.4-3). The forward and back boundaries are given by $\delta'_f(\beta)$ and $\delta'_b(\beta)$, respectively. With these definitions we write the PSF as

$$P(\delta', \beta) = \begin{cases} 0 & |\beta| > 2a \\ 0 & \delta' < \delta'_f(\beta) \\ F[\delta' - \delta'_f(\beta)] & \delta'_f(\beta) \le \delta' < \delta'_b(\beta) \\ F[\delta' - \delta'_f(\beta)] - F[\delta' - \delta'_b(\beta)] & \text{(otherwise)} \end{cases} \quad (4.4\text{-}1)$$

where

$$
\begin{aligned}
F(\xi) \;=\; & 1 - (1 + a_1 + a_2)e^{-c_1\xi} \\
& + e^{-6.35465\xi}[a_1\cos(1.90282\xi) + b_1\sin(1.90282\xi)] \\
& + e^{-4.61598\xi}[a_2\cos(5.83072\xi) + b_2\sin(5.83072\xi)]
\end{aligned}
\qquad (4.4\text{-}2)
$$

and

$$
a_1 = 1.84205 \qquad a_2 = -0.22502
$$
$$
b_1 = 1.47034 \qquad b_2 = 0.45904
$$
$$
c_1 = 1.98412
$$

The centroid of the PSF is derived in Smith (1994) and is approximately 1.0^o from the optical axis. This shift is denoted in Figure 4.4-3 and a new angle δ is defined relative to the centroid. To evaluate the PSF we determine δ and then set $\delta' = \delta + \Delta\delta$ where $\Delta\delta$ is the shift from the optical axis to the centroid.

4.4.2.2. Geometry of the Point Spread Function

The scanner footprint geometry is given in Figure 4.4-2. The optical field-of-view (FOV) is a truncated diamond (or hexagon) and is 1.3^o in the along-scan direction and 2.6^o in the across-scan direction. The effective field-of-view (or footprint) is given by the PSF and is shown as an ellipse. A point within the footprint is located by β and δ. The cone angle α (or nadir angle) determines the location of the footprint centroid on the Earth. If $\alpha = 0$, the footprint is at nadir. The viewing zenith angle θ is a direct result of the satellite altitude h, the Earth radius r_E, and the cone angle α. The surface distance l and the Earth central angle γ between nadir and the centroid are also a result of the viewing geometry. In Figure 4.4-2 we have denoted the length of the FOV by Δl.

Figure 4.4-3 gives three CERES FOVs. The shaded area is the optical FOV. Note that only half of the FOV is given since it is symmetrical about the scan line. We have placed the origin at the centroid of the PSF which trails the optical axis by about 1.0 degree. This is the lag that is inherent in the system. About the PSF centroid we have drawn the outlines of the half-power cutoff and the full 95-percent energy cutoff. All of the pertinent dimensions are given.

Table 4.4-1 and Table 4.4-2 give numerical values for the TRMM and EOS satellites. Table 4.4-1 presents the orbital characteristics and a summary of the footprint sizes. The largest footprint determines how close we can get to the end of the 500-km swath of imager data before we need to stop and extend the imager data. For TRMM the optical FOV projected onto the surface at nadir is 8 km long in the scan direction and 16 km wide. Frequently this footprint is referenced by its equivalent area circle with a diameter of approximately 10 km. The optical FOV, however, is spread over the surface according to the point spread function as discussed above. We can also project the PSF on the surface at nadir. If we truncate the PSF at the half-power point, then the footprint is 9×13 km. If we truncate the PSF so that 95-percent energy is retained, then

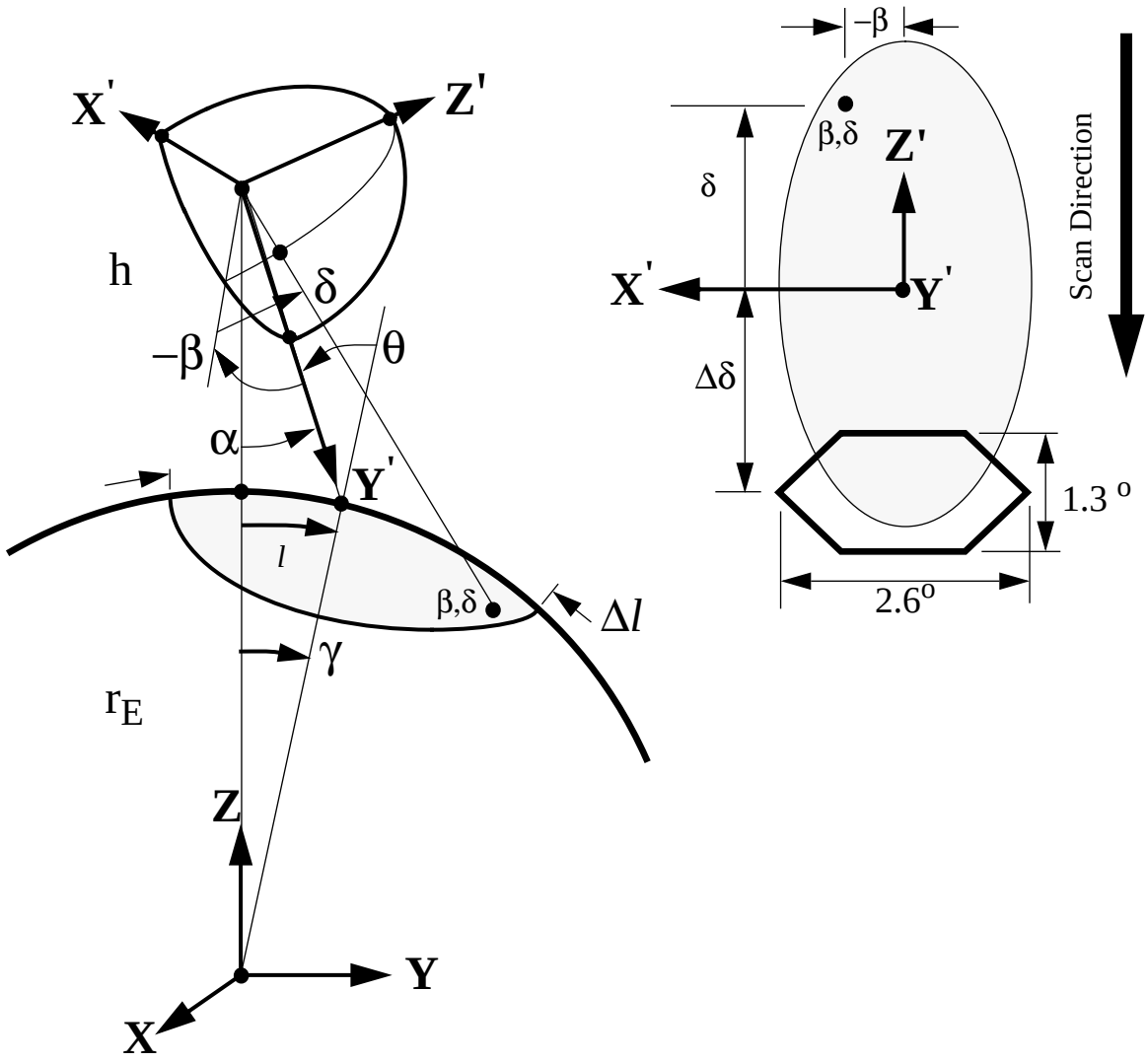

Figure 4.4-2. Scanner Footprint Geometry

the footprint grows to 16×16 km. Normally radiance measurements are inverted to flux at the TOA only out to a viewing zenith angle of 70^o. At this point the TRMM scanner FOV has grown to 116×38 km. The along scan direction increases much more rapidly than the cross scan direction because of the shallow angles. Table 4.4-2 gives footprint sizes for various viewing geometry for both the TRMM and EOS satellites.

4.4.2.3. Evaluation of the Point Spread Function

At each imager pixel cloud parameters are defined. We will need the value of the PSF over the footprint to form weighted averages of these cloud parameters. We now examine the geometry of this calculation.

The colatitude and longitude of the PSF centroid is recorded on the SSF product along with the

CERES footprint radiometric data and other geometric parameters. On the SSF is recorded the cone angle α and its time rate of change $\dot{\alpha}$ (Figure 4.4-5). Recall that we need to determine the along-scan angle δ and the cross-scan angles β of an imager pixel to evaluate the PSF. Referring to Figure 4.4-2, we need to form an axis system at the satellite. If we define $\hat{X}_{sat}$ as the unit vector to the satellite, then we can define the $\hat{X}'$, $\hat{Y}'$, $\hat{Z}'$ axis with the $\hat{Y}'$ axis pointing toward the centroid, the $\hat{X}'$ axis perpendicular to $\hat{Y}'$ and $\hat{X}_{sat}$, and $\hat{Z}'$ completing the triad. We then determine δ and β of the imager pixel relative to the $\hat{X}'$, $\hat{Y}'$, $\hat{Z}'$ axis.

The colatitude and longitude of the footprint centroid at the surface is from the SSF product. Working in the Greenwich Meridian, Earth equator coordinate system (Figure 4.4-4), we have

$$\begin{aligned} x_{cen} &= \sin\Theta_{cen}\cos\Phi_{cen} \\ y_{cen} &= \sin\Theta_{cen}\sin\Phi_{cen} \\ z_{cen} &= \cos\Theta_{cen} \end{aligned} \tag{4.4-3}$$

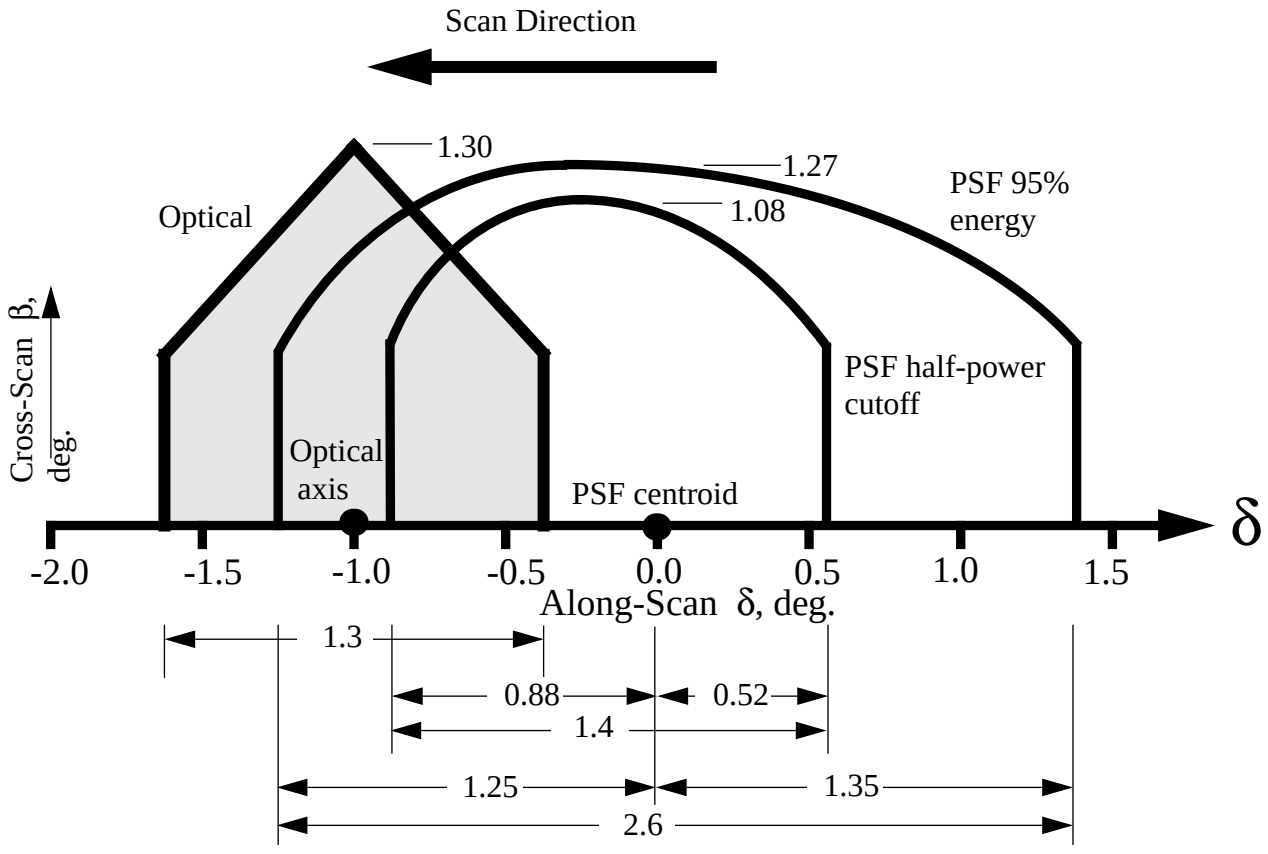

Figure 4.4-3. CERES Field-of-Views

Table 4.4-1: Orbital and FOV Characteristics

		TRMM	EOS
h	Altitude of spacecraft, km	350	705
r_E	Radius of surface, km.	6367	6367
α_h	Cone angle at horizon, deg.	71.4	64.2
γ_h	Earth central angle (ECA) at horizon, deg.	18.6	25.8
P	Period, minute	91.4	98.7
Optical hexagonal footprint. Center at nadir.		8×16[a] ≈10 circle	16×32 ≈20 circle
PSF half-power cutoff. Centroid at nadir.		9×13	17×27
PSF 95% energy cutoff. Centroid at nadir.		16×16	32×31
PSF 95% energy cutoff. Centroid at θ[b] = 70°.		116×38	212×71
PSF 95% energy cutoff. Centroid at $\theta = 75°$.		186×47	328×82
PSF 95% energy cutoff. Limit of Earth view at horizon.		507×63	660×97
PSF half-power cutoff. Centroid at $\theta = 75°$.		103×40	182×69

a. Footprint size in along scan length × perpendicular to scan width in km.
b. θ is viewing zenith at the surface.

Table 4.4-2: Footprint Sizes

TRMM					EOS				
δ	β	θ	l	Δl	δ	β	θ	l	Δl
Optical hexagonal footprint at nadir, $\alpha = 0^o$					Optical hexagonal footprint at nadir, $\alpha = 0^o$				
-0.35	0	-	-2		-0.35	0	-	-4	
-1.65	0	-	-10	8	-1.65	0	-	-20	16
-1.00	±1.30	-	-	16	-1.0	±1.30	-	-	32
PSF half-power cutoff at nadir, $\alpha = 0^o$					PSF half-power cutoff at nadir, $\alpha = 0^o$				
-0.88	0	0.9	5.4		-0.88	0	1.0	10.8	
0.52	0	0.5	-3.2	9	0.52	0	0.6	-6.4	17
0	1.08	1.1	6.6	13	0	1.08	1.2	13.3	27
PSF 95% energy cutoff at nadir, $\alpha = 0^o$					PSF 95% energy cutoff at nadir, $\alpha = 0^o$				
-1.25	0	1.3	7.6		-1.25	0	1.4	15.4	
1.35	0	1.4	8.2	16	1.35	0	1.5	16.6	32
0	1.27	1.3	7.8	16	0	1.27	1.4	15.6	31
PSF 95% energy cutoff Centroid at $\theta = 70^o$, $\alpha = 62.96^o$, $\gamma = 7.04^o$					PSF 95% energy cutoff Centroid at $\theta = 70^o$, $\alpha = 57.78^o$, $\gamma = 12.22^o$				
-1.25	0	71.8	841.8		-1.25	0	72.2	1468.7	
0	0	70.0	781.6		0	0	70.0	1357.7	
1.35	0	68.1	725.6	116	1.35	0	67.7	1256.7	212
0	1.27	70.0	19.4	38	0	1.27	70.0	35.3	71
PSF 95% energy cutoff Centroid at $\theta = 75^o$, $\alpha = 66.29^o$, $\gamma = 8.71^o$					PSF 95% energy cutoff Centroid at $\theta = 75^o$, $\alpha = 60.42^o$, $\gamma = 14.58^o$				
-1.25	0	77.1	1067.7		-1.25	0	77.9	1800.9	
0	0	75.0	967.8		0	0	75.0	1621.1	
1.35	0	72.9	881.7	186	1.35	0	72.3	1472.6	328
0	1.27	75.0	23.3	47	0	1.27	75.0	40.9	82
PSF 95% energy cutoff Limit of Earth view at horizon $\alpha = \alpha_h - 1.65^o = 69.75^o$					PSF 95% energy cutoff Limit of Earth view at horizon $\alpha = \alpha_h - 1.65^o = 62.55^o$				
-1.25	0	85.9	1660.6		-1.25	0	85.3	2387.0	
0	0	81.8	1338.5		0	0	80.3	1971.4	
1.35	0	78.8	1153.5	507	1.35	0	76.7	1726.8	660
0	1.27	81.8	31.4	63	0	1.27	80.3	48.5	97
PSF half-power cutoff at $\theta = 75^o$, $\alpha = 66.29^o$					PSF half-power cutoff at $\theta = 75^o$, $\alpha = 60.42^o$				
-0.88	0	76.5	1035.6		-0.88	0	77.0	1741.8	
0	0	75.0	967.8		0	0	75.0	1621.1	
0.52	0	74.2	932.5	103	0.52	0	73.9	1559.6	182
0	1.08	75.0	19.8	40	0	1.08	75.0	34.8	69

The unit vector to the satellite $\hat{X}_{sat}$ and to an imager pixel $\hat{X}_{imag}$ are determined from their colatitude and longitude in the same way.

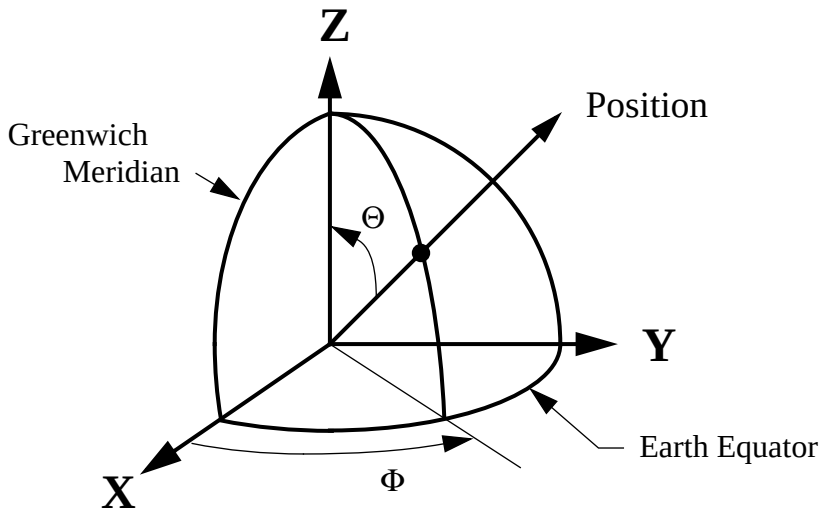

Figure 4.4-4. Colatitude and Longitude Angles

The viewing geometry for the centroid of the PSF is given in Figure 4.4-5. The Earth central angle γ between the satellite and the centroid is

$$\cos\gamma = \hat{X}_{sat} \bullet \hat{X}_{cen} \qquad 0 \le \gamma \le 90° \tag{4.4-4}$$

The slant range, ρ, from the satellite to the centroid is from the law of cosines or

$$\rho = [(r_E + h)^2 + r_E^2 - 2(r_E + h)r_E\cos\gamma]^{\frac{1}{2}} \tag{4.4-5}$$

From Figure 4.4-2 and Figure 4.4-5 we have

$$(r_E + h)\hat{X}_{sat} + \rho\hat{Y}' = r_E\hat{X}_{cen}$$

or

$$\hat{Y}' = \frac{r_E\hat{X}_{cen} - (r_E + h)\hat{X}_{sat}}{\rho} \tag{4.4-6}$$

and

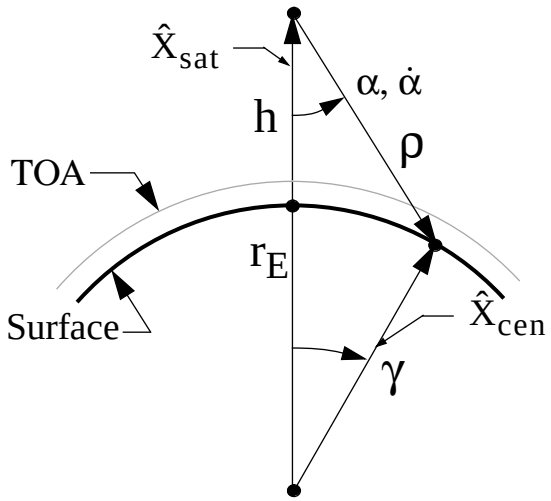

Figure 4.4-5. Viewing Geometry

$$\hat{X}' = \frac{\hat{Y}' \times \hat{X}_{sat}}{\left\| \hat{Y}' \times \hat{X}_{sat} \right\|} \qquad (4.4\text{-}7)$$

$$\hat{Z}' = \hat{X}' \times \hat{Y}'$$

We now derive a unit vector from the satellite to an imager pixel on the surface in the same way. By substituting $\hat{X}_{imag}$ for $\hat{X}_{cen}$ in (4.4-4), (4.4-5), and (4.4-6), we derive the view vector to the imager pixel, say $\hat{Y}'_{imag}$, so that

$$\hat{Y}'_{imag} \bullet \hat{Z}' = \cos(90° - \delta)$$

and

$$\frac{\hat{Z}' \times \hat{Y}'_{imag}}{\left\| \hat{Z}' \times \hat{Y}'_{imag} \right\|} \bullet \hat{Y}' = \cos(90° + \beta)$$

or

$$\begin{aligned} \sin\delta &= \hat{Y}'_{imag} \bullet \hat{Z}' && -90° \le \delta \le 90° \\ \sin\beta &= -\frac{\hat{Z}' \times \hat{Y}'_{imag}}{\left\| \hat{Z}' \times \hat{Y}'_{imag} \right\|} \bullet \hat{Y}' && -90° \le \beta \le 90° \end{aligned} \tag{4.4-8}$$

and finally we evaluate $P(\delta', \beta)$ from (4.4-1) where $\delta' = \delta + \Delta\delta$ and $\Delta\delta$ is the shift from the optical axis to the centroid. If $P(\delta', \beta) \ge P_{95\%}$, then the imager pixel is within the CERES footprint.

The geometry in Figure 4.4-2 and the discussion so far has assumed the scan is inward, toward nadir, so that $\dot{\alpha} < 0$ and the tail of the PSF is outward. For this case δ is positive in the $\hat{Z}'$ direction. If the scan is outward so that $\dot{\alpha} > 0$ and the tail of the PSF is inward, then we must reverse the sign of δ from (4.4-8) so that $\delta' = -\delta + \Delta\delta$. If $\dot{\alpha} = 0$, then the scan is fixed and we use a "static PSF" instead of the PSF defined by (4.4-1). A reasonable "static PSF" is a constant response over the optical FOV. We will also encounter a retrace scan during the short scan mode (see Figure 1-7) where $|\dot{\alpha}| = 249.8°/\text{sec}$. The data for this case will not be processed because of the FOV growth.

We have evaluated the PSF at the imager pixel starting with its surface colatitude and longitude. The CERES centroid is also located at the surface by its colatitude and longitude in the same way as the imager. Thus, for cross-track scanning the locations align well. However, there is a location error when the imager is scanning cross-track and the CERES is scanning at another azimuth. The scanners actually sense the radiation along the slant path defined by its viewing zenith angle. Although both instruments view the same surface point, they will view different points at an altitude above the surface. Thus, the observed cloud fields will be slightly different and the error will be a function of cloud height and spatial autocorrelation. This problem is minimal since the azimuth scanning data is mainly for the angular distribution model (ADM) development. If the location errors are random with mean zero, then the errors will not cause an ADM bias error but only an increase in variance which will require slightly more data to overcome.

4.4.2.4. Spatial Ordering of CERES Data

The CERES data have been spatially ordered in Subsection 1.0 to facilitate the collocation of the imager data and the CERES footprint. The rotating azimuth plane scanner has the capability of viewing 1000 km forward along the groundtrack and 3.3 seconds later viewing 1000 km backward along the groundtrack. This distance plus the size of the footprints would require about 2500 km of imager data to be available for collocating at one time. To circumvent this problem, the CERES data have been spatially ordered along the groundtrack according to their along-track angle.

The along-track angle γ_{at} and the cross-track angle γ_{ct} define the location of the CERES footprint relative to the orbit plane and relative to the start of the one hour SSF product (see Figure 4.4-6). These footprint location angles are determined from the orbital geometry. Let us define the time at the start of the one hour SSF product as t_o. The position of the satellite at t_o is

defined as $\hat{X}_o$. The colatitude and longitude of the satellite at t_o are defined by Θ_o and Φ_o as in Figure 4.4-4 so that the position components are

$$\begin{aligned} x_o &= \sin\Theta_o \cos\Phi_o \\ y_o &= \sin\Theta_o \sin\Phi_o \\ z_o &= \cos\Theta_o \end{aligned} \tag{4.4-9}$$

where $\hat{X}_o$ is expressed in the Earth equator, Greenwich meridian coordinate system at the hour start, t_o. We freeze this coordinate system at t_o so that it does not rotate. This will be our basic, inertial coordinate system. The satellite inertial velocity at t_o is given by ephemeris data $\dot{x}_o, \dot{y}_o, \dot{z}_o$. The unit angular momentum vector is perpendicular to the orbit plane and is given by

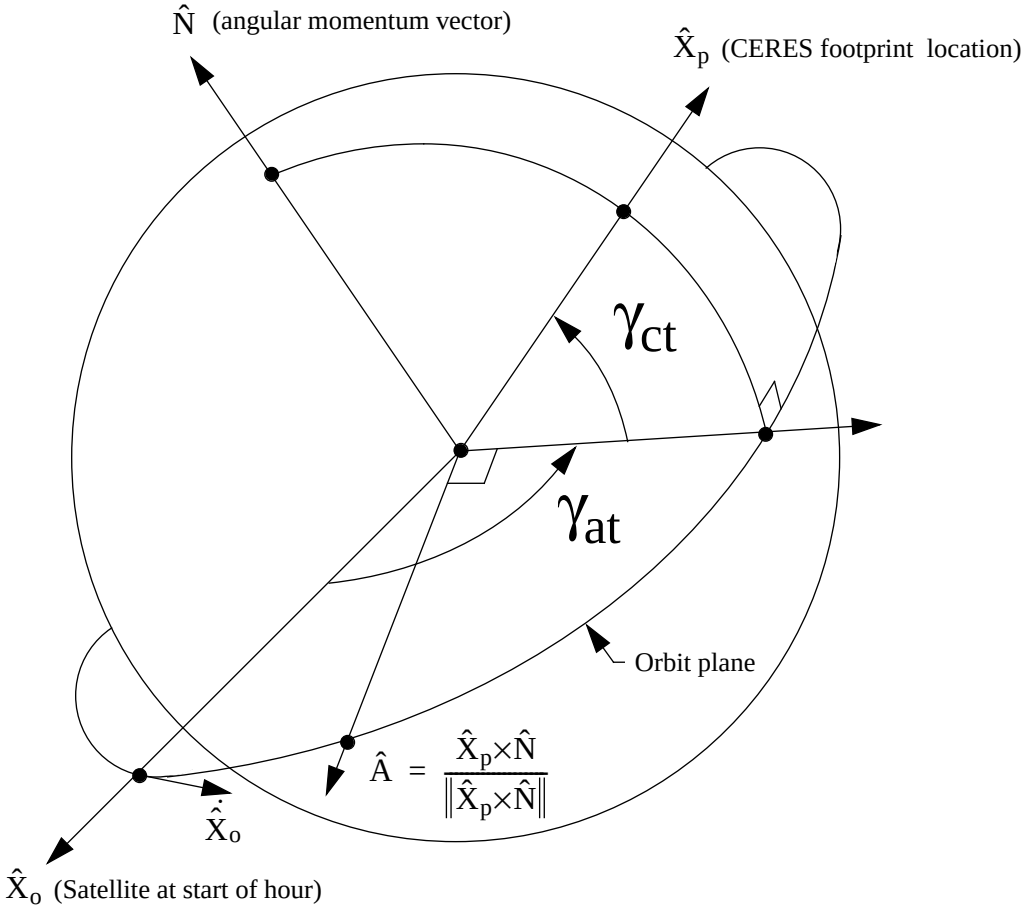

Figure 4.4-6. Along-track and Cross-track Angles

$$\hat{N} = \frac{\hat{X}_o \times \dot{\hat{X}}_o}{\left\| \hat{X}_o \times \dot{\hat{X}}_o \right\|} \tag{4.4-10}$$

where $\left\| \vec{X} \right\|$ denotes the magnitude of $\vec{X}$, or

$$\left\| \vec{X} \right\| = \sqrt{x^2 + y^2 + z^2}. \tag{4.4-11}$$

The position of a footprint $\hat{X}_p$ at time t is given by Θ_p, Φ_p. This position is in the Earth equator, Greenwich meridian coordinate system at time t. The position in our basic, inertial coordinate system is

$$\begin{aligned} \Delta t &= t - t_o \\ \Delta\Phi &= \omega_E \Delta t \end{aligned} \tag{4.4-12}$$

$$\begin{aligned} x_p &= \sin\Theta_p \cos(\Phi_p + \Delta\Phi) \\ y_p &= \sin\Theta_p \sin(\Phi_p + \Delta\Phi) \\ z_p &= \cos\Theta_p \end{aligned} \tag{4.4-13}$$

where the rotational rate of the Greenwich meridian is $\omega_E = 0.004178$ deg/sec.

The cross-track angle is given by

$$\hat{X}_p \bullet \hat{N} = \cos(90° - \gamma_{ct})$$

or

$$\sin\gamma_{ct} = \hat{X}_p \bullet \hat{N} \qquad -90° \le \gamma_{ct} \le 90° \tag{4.4-14}$$

The along-track angle is given by

$$\hat{A} = \frac{\hat{X}_p \times \hat{N}}{\left\| \hat{X}_p \times \hat{N} \right\|}$$

$$\hat{A} \bullet \hat{X}_o = \cos(\gamma_{at} - 90°)$$

$$\hat{X}_o \times \hat{A} \bullet \hat{N} = \sin(\gamma_{at} - 90°)$$

or

$$\sin\gamma_{at} = \hat{A} \bullet \hat{X}_o$$
$$\cos\gamma_{at} = -\hat{X}_o \times \hat{A} \bullet \hat{N} \qquad 0° \le \gamma_{at} < 360° \quad (4.4\text{-}15)$$

The SSF product contains one hour of CERES footprint data for one scanning radiometer. Each footprint is a separate record and is organized spatially along the groundtrack with increasing along-track angle. The reference point of the data on the one hour SSF is the nadir position of the satellite on the groundtrack when the hour starts. This point is defined as 0° along-track angle. Measurements made after this "initial time" that look backwards and have footprints with along-track angle near 360^o are included on the SSF hour product with negative along-track angles. Also, footprints are included that view beyond the satellite nadir at hour end. All CERES data is ordered in increasing along-track angle including both fixed azimuth plane scan (FAP) and rotating azimuth plane scan (RAP).

4.4.2.5. Geometry of Collocation

The time of observation and the size of the CERES footprint will vary greatly, but the locations of the CERES footprints are well behaved. Figure 4.4-7 illustrates this geometry. Consider the three contiguous numbered footprints. The first footprint represents the maximum size footprint. According to Table 4.4-2 a CERES footprint directed forward along the groundtrack from the TRMM orbit and at a shallow viewing zenith angle of 75^o extends from 100 km forward of the PSF centroid to 86 km backwards of the centroid and is 47 km wide. The measurement is made when the satellite is 968 km back from the centroid and 2.2 minutes away. Therefore our field of imager data must be at least 186 km in length. A reasonable swath length of imager data is 500 km which will allow many CERES footprints to be collocated. After all of the imager pixels within this footprint are located and the cloud statistics determined, we move to the next CERES footprint denoted by "2". This footprint was obtained by viewing off the groundtrack when the satellite was beyond the area of interest. Its shape is skewed which makes the collocation more complex. The next CERES footprint denoted by "3" is a nadir viewing footprint. From Figure 4.4-7 we see that spatial ordering gives varying footprint sizes and times of observation, but has footprints that are close to each other.

We proceed along the groundtrack and collocate footprints until we are within about 100 km of the end to the 500 km swath of imager data. At that point we drop data at the back of the swath and add new data on the forward part of the swath, analyze this new swath, and then start the collocation process where we left off. This continues until we are again within 100 km of the end of the swath.

The geometry of the process of locating the actual imager pixels within the CERES footprint is shown in Figure 4.4-8. Knowing the along-track and cross-track angle of the centroid of a CERES footprint (represented by the open circle in Figure 4.4-8), we can easily locate the nearest imager pixel (denoted by the number 1 solid circle). Since the CERES measurement time t_c and the imager measurement time t_i are different, the CERES footprint will have moved from its original location due to the rotation of the Earth. For the moment we will assume pixel 1 is within the footprint at time t_i. The test for a pixel to be within the footprint is to determine the value of the PSF and test against the 95-percent energy value. Next, we move outward to pixel 2 and evaluate

the PSF at this point to determine if the pixel is within the footprint. We proceed in this manner until we reach pixel 12 that is outside the footprint. We then return to pixel 1 and proceed inward until pixel 14 is reach. This completes one row of imager pixels. We find the center pixel 5 and step to the next row. This is denoted by pixel 15. By finding the center pixel we stay within the footprint even for the skewed case. From pixel 15 we step outward and then inward until we complete the row. This process is continued until the step from center is outside the footprint shown as pixel 257. Returning to the center of the first row, we step to pixel 258 and continue until all the imager pixels are located. It is possible for the PSF centroid at t_c to be outside the footprint at t_i. In this case we search eastward for an imager pixel with a colatitude and longitude that is near the PSF centroid. If $t_c<t_i$, search eastward. Otherwise, search westward.

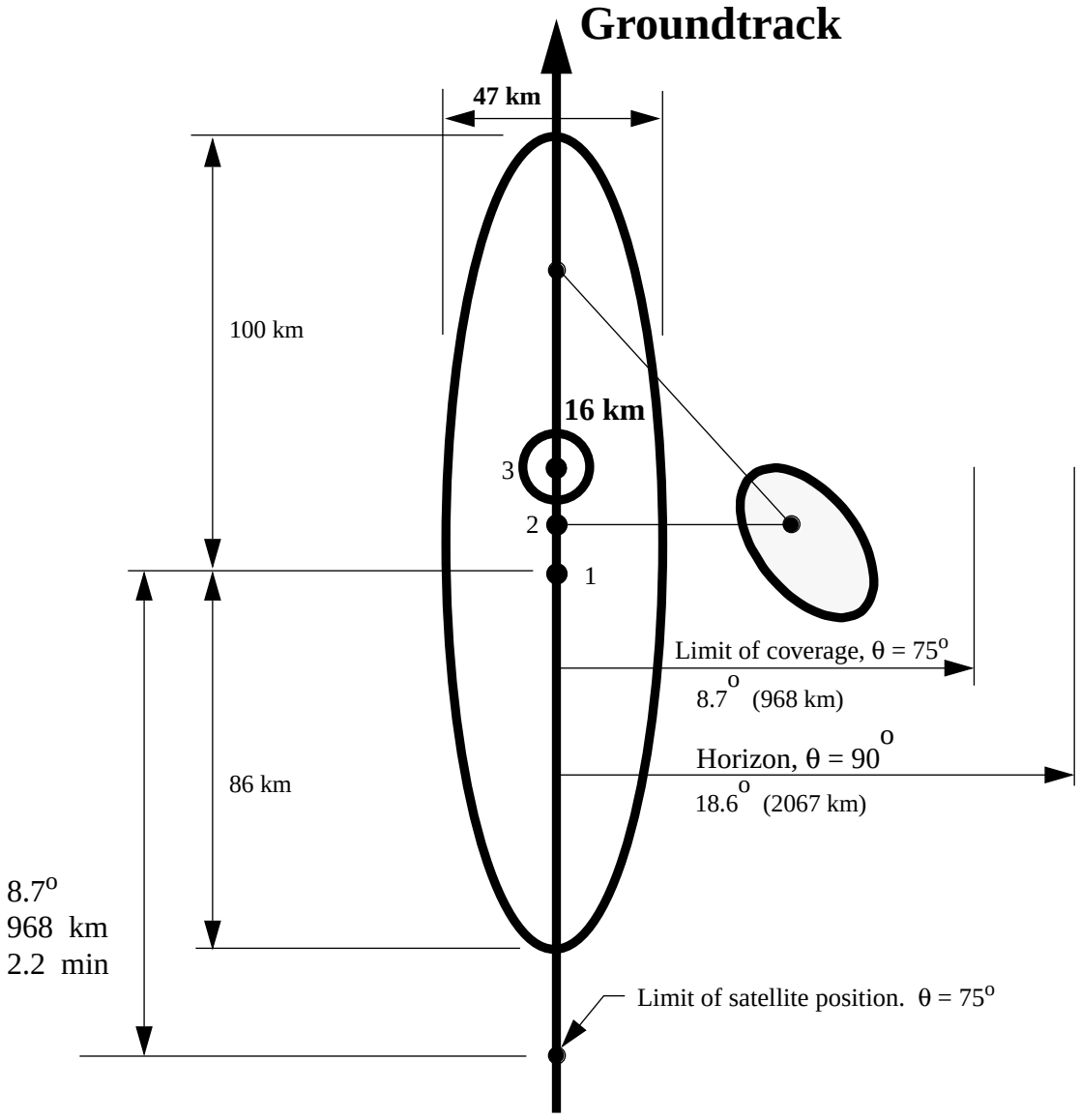

Figure 4.4-7. Spatial Ordering of CERES Footprints

In general the imager does not scan to the horizon but restricts its scan to a swath along the groundtrack. Thus, we will encounter the case where the CERES footprint is only partially covered by imager pixels. In this case we integrate the PSF over the area of the footprint that is covered and accept the partial coverage if the energy is 75 percent or greater instead of the normal 95-percent energy.

This section contains a conceptual discussion of collocation for uniformly spaced imager data. In general the imager data is not uniformly spaced and angular bins must be used to integrate over the CERES footprint (see section 4.4.2.6).

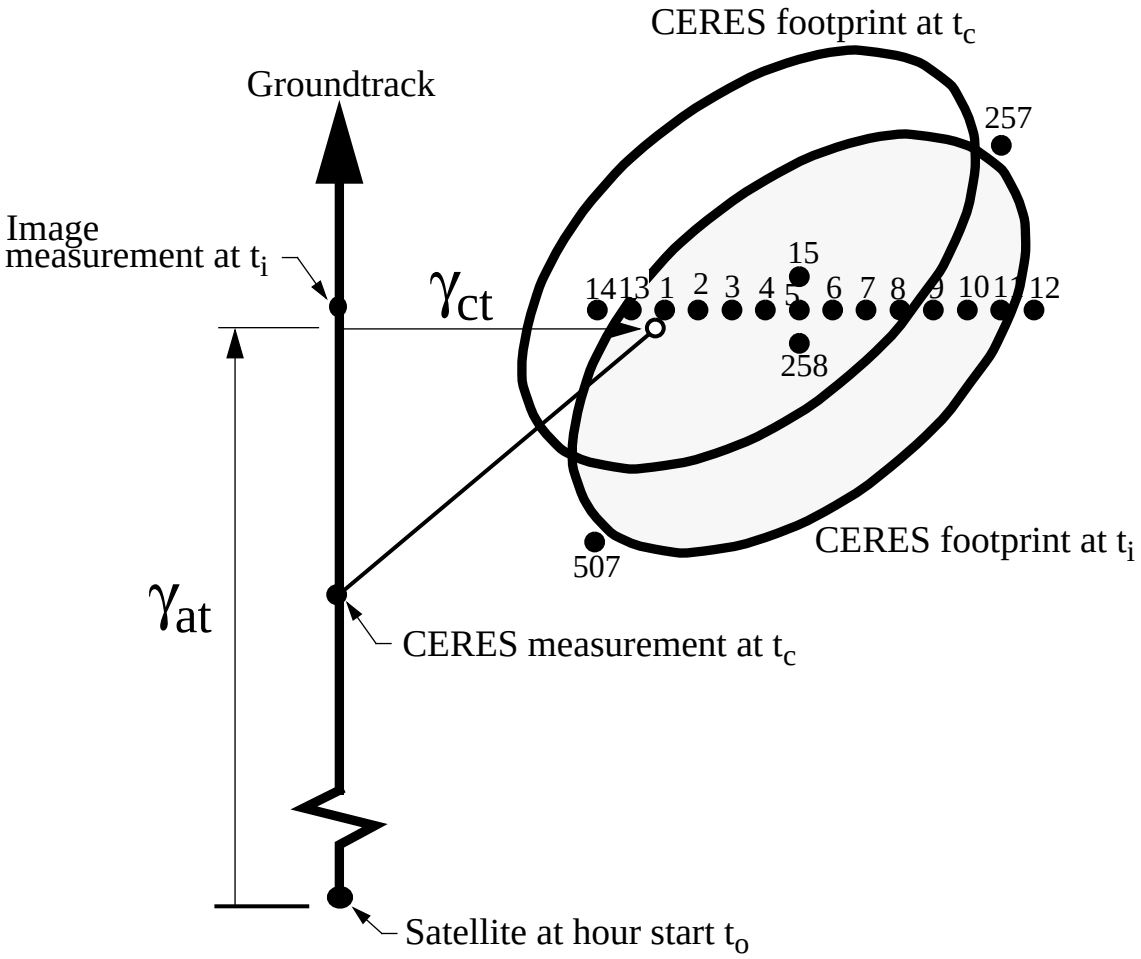

Figure 4.4-8. Collocating Imager Pixels and CERES Footprints

4.4.2.6. Integration over the CERES FOV

We will need to integrate over the CERES FOV to determine the average cloud properties and area coverage. If we define x as a general cloud parameter over the 95% energy FOV (Figure 4.4-3), then the weighted average value of x is given by

$$\bar{x} = \frac{\int_{FOV} P(\delta, \beta) x(\delta, \beta) \cos\delta d\beta d\delta}{\int_{FOV} P(\delta, \beta) \cos\delta d\beta d\delta} \tag{4.4-16}$$

where $P(\delta, \beta)$ is the point spread function (PSF) (4.4-1) and δ and β are the coordinates of a point in the FOV (Figure 4.4-2). The value of x is known only at discrete imager pixels. We denote the values within the FOV by $x(\delta_k, \beta_k) \equiv x_k$ where k = 1,2,...,K. In general these x_k's will not be uniformly spaced over the FOV so that we must average over smaller sections of the FOV or a sub-grid and then integrate. Let us define a δ–β grid that matches the imager sampling at nadir (see sketch). Ideally, this grid would give one imager sample per grid area or angular bin. For TRMM we have h = 350 km and for VIRS Δl = 2 km so that $\Delta\delta = \tan^{-1}\left(\frac{\Delta l}{h}\right) = 0.33$ deg .

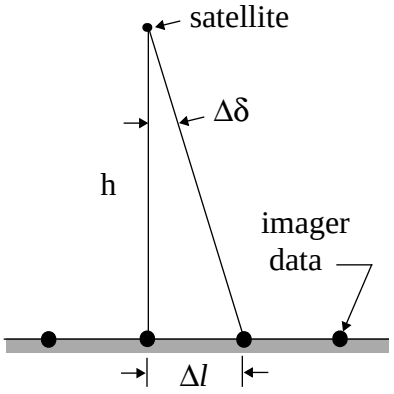

For EOS-AM we have h = 705 km and for MODIS Δl = 1 km so that $\Delta\delta$ = 0.08 deg. Thus, for TRMM we define a δ–β grid where the bin size is $\Delta\delta = 0.33$ deg and $\Delta\beta = 0.33$ deg and assume $x(\delta,\beta)$ is constant within a bin. We can now express the average value of x from (4.4-16) as

$$\bar{x} = \frac{\sum_{i,j} w_{ij} x_{ij}}{\sum_{i,j} w_{ij}} \tag{4.4-17}$$

where the weight w_{ij} is the integral of the PSF over an angular bin or

$$w_{ij} \equiv \int_{\delta=\delta_i}^{\delta=\delta_i+\Delta\delta} \int_{\beta=\beta_i}^{\beta=\beta_i+\Delta\beta} P(\delta,\beta)\cos\delta d\beta d\delta \qquad (4.4\text{-}18)$$

and x_{ij} is the arithmetric mean of all the $x(\delta_k, \beta_k)$ in the angular bin such that $\delta_i < \delta_k \le \delta_i + \Delta\delta$ and $\beta_i < \beta_k \le \beta_i + \Delta\beta$. The δ–β grid and values of w_{ij} are given in Figure 4.4-9 for half the FOV. We have taken the FOV to be defined by $-1.32^o<\delta\le 1.32^o$ and $-1.32^o<\beta\le 1.32^o$ which approximates the 95% energy FOV in Figure 4.4-3. The integral over the square FOV is given by $\sum_{ij} w_{ij} = 0.9634$ which is slightly greater than 95% energy.

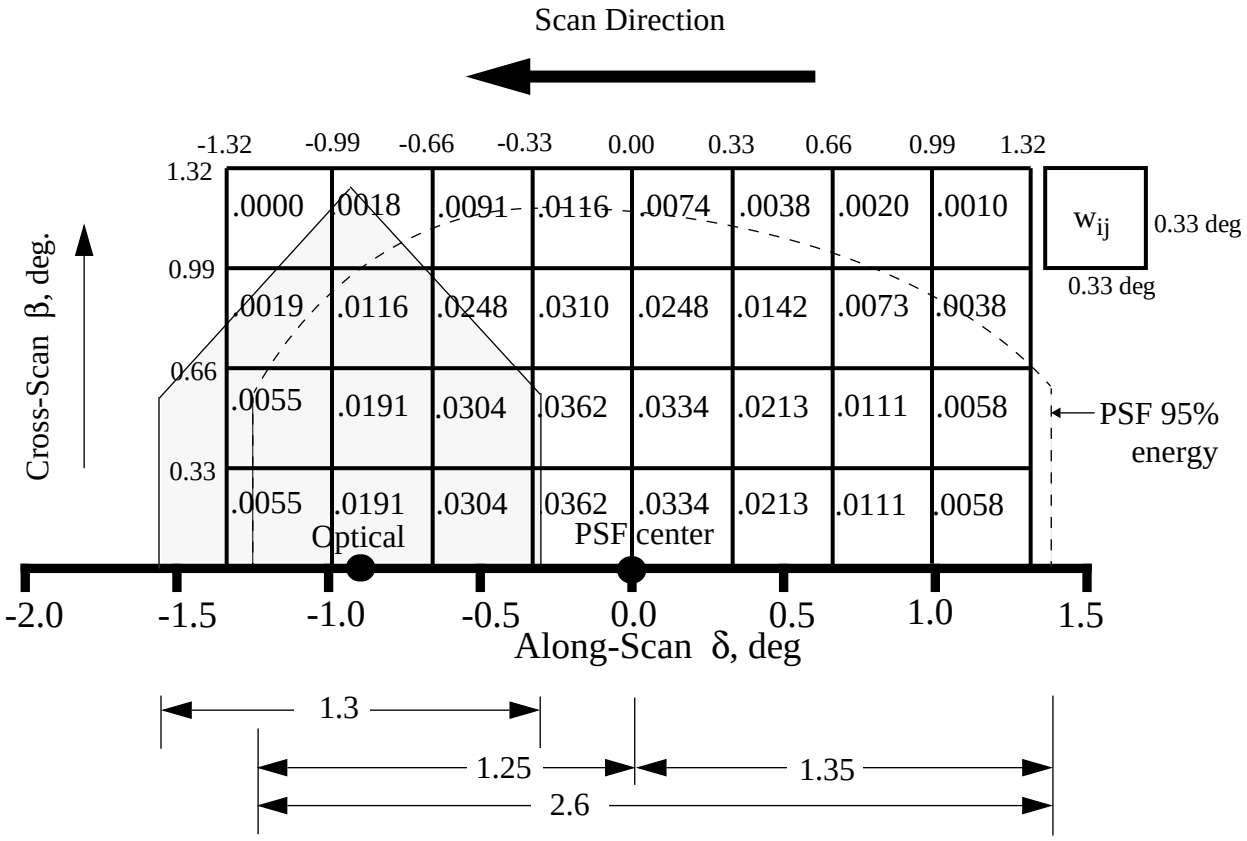

Figure 4.4-9. CERES Field-of-View Angular Grid

So far we have made mention of only the centroid of the PSF. We now consider three measures of the central tendency. For the PSF in (4.4-1) the mean (centroid) is 0.96 deg from the optical axis, the mode (maximum P) is 0.90 deg and the median (50 percentile) is 0.89 deg. Since the

scanner center location will ultimately be fine tuned with an empirical coastline detector (Hoffman et al., 1987) and alignment with the imager navigation, the PSF centroid will be used as the center of the PSF and δ and β are referenced to this point. Thus, for Figure 4.4-3, the optical axis is at δ = -0.96.

We also need to determine the imager area coverage. The imager data, in general, does not extend to the limb so that some CERES footprints will have only partial imager coverage. Other angular bins will be empty because of missing imager data. We can determine the imager area coverage by (4.4-17) where x_{ij} = 1 if the (i,j) angular bin contains imager data and x_{ij} = 0 otherwise. If the imager coverage is less than 75%, then we disregard the CERES footprint.

4.4.2.7. Cloud Statistics over a CERES FOV

For every imager pixel the parameters listed in Table 4.4-3 are determined (see Subsystems 4.1, 4.2, 4.3). If the number of cloud layers (parameter #1) is 0, then the pixel is clear and #21 - #42 are meaningless. If there is one cloud layer, then #21 - #31 contain the cloud properties. If there are two layers, then all parameters have meaning and cloud layer 1 is the lower cloud and cloud layer 2 is the higher cloud. And finally, if #1 is -1 (which is a special use of the parameter), then we disregard the pixel altogether.

Since the cloud field is considered constant over an angular bin (see Figure 4.4-3), we must declare each bin either clear, a one layer cloud, or a two layer cloud system. We cannot make this

Table 4.4-3. Imager Pixel Parameters

General	Cloud layer 1 (low)	Cloud layer 2 (high)
1. Number of cloud layers (-1, 0, 1, or 2)	21. Visible optical depth	32. Visible optical depth
2. Cloud fraction (0-1.0)	22. Infrared emissivity	33. Infrared emissivity
3. Time of imager observation	23. Water path	34. Water path
4. Imager colatitude and longitude	24. Top pressure	35. Top pressure
5. Altitude of surface above sea level	25. Effective* pressure	36. Effective* pressure
6. Surface type index	26. Effective temperature	37. Effective temperature
7. Imager viewing zenith angle	27. Effective height	38. Effective height
8. Imager solar zenith angle	28. Bottom pressure	39. Bottom pressure
9. Imager relative azimuth angle	29. Particle radius	40. Particle radius
10. Imager channel identifier (5 items)	30. Particle phase (0-ice or 1-water)	41. Particle phase (0-ice or 1-water)
11. Imager radiance for #10 (5 items)	31. Vertical Aspect ratio	42. Vertical Aspect ratio
12. Sunglint index		
13. Snow/Ice index		
14. Smoke index		
15. Fire index		
16. Shadowed index		
17. Total aerosol vis. optical depth, clear		
18. Total aerosol effective radius, clear		
19. Imager-based surface skin temperature		
20. Algorithm notes		

* Effective as viewed from space or cloud top if optically thick and cloud center if optically thin.

choice until all pixels are accumulated. Thus, we will need three sums for each bin. The first sum is for clear pixels and records parameters #1 - #20 along with the number of pixels found. The second sum is for pixels with one layer clouds and records parameters #1 - #31. The third sum is for pixels with two layer clouds and records parameters #1 - #42. After all pixels within the footprint have been found and recorded, the sum with the most pixels is selected and the other two sums are discarded. If clear and one layer tie for the most pixels, then one layer is selected over a contaminated clear scene. If one layer and two layers tie for the most pixels, then one layer is selected for simplicity. If clear and two layers tie for the most pixels, then there is confusion and all three sums are discarded and the bin is considered empty. Most pixels within a bin should agree on the cloud layer so that this procedure will eliminate odd or erroneous pixels. The final result is one set of average cloud parameters (Table 4.4-3) for each bin with #1 equal to -1, 0, 1 or 2.

Clouds will be defined as being in one of four height categories (Figure 4.4-10) by their effective pressure (#25 and #36). Category 1 (low clouds) corresponds to a cloud pressure greater than 700 hPa, category 2 (lower middle clouds) corresponds to a cloud pressure between 700 and 500 hPa, etc. In general a single footprint can contain clear areas and clouds in all four categories. However, we will restrict clouds within a single footprint to two layers and assign each cloud layer to the height category which contains the layer average pressure. Layer 1 is defined as the lowest layer and we will assign it to category A where A could be 1, 2, 3, or 4. If there is a second layer, then layer 2 is the highest layer and we assign it to category B where B could be 2, 3, or 4, but not the same as category A. The mean cloud data within an angular bin is defined as being in categories A and B. It is possible, however, for the effective pressure of a given angular bin to be outside of categories A and B, but recall we have defined layers and assigned each layer to the category containing its mean.

We also determine an overlap condition for each angular bin as defined in Table 4.4-4. Note that clear areas have no clouds, but are still define as one of the 11 cloud overlap conditions, or the condition of no clouds. Thus, although there are 11 possible overlap conditions in general, there

Table 4.4-4. Eleven Cloud Overlap Conditions

Index	Definition	Symbol	
No layer			
1	clear (no clouds)	CLR	0
One layer			
2	low cloud only (cloud effective pressure > 700 hPa)	L	1
3	lower middle cloud only (700 ≥ eff. pressure > 500 hPa)	LM	2
4	upper middle cloud only (500 ≥ eff. pressure > 300 hPa)	UM	3
5	high cloud only (eff. pressure ≤ 300 hPa)	H	4
Two layers			
6	high cloud over upper middle cloud	H/UM	43
7	high cloud over lower middle cloud	H/LM	42
8	high cloud over low cloud	H/L	41
9	upper middle cloud over lower middle cloud	UM/LM	32
10	upper middle cloud over low cloud	UM/L	31
11	lower middle cloud over low cloud	LM/L	21

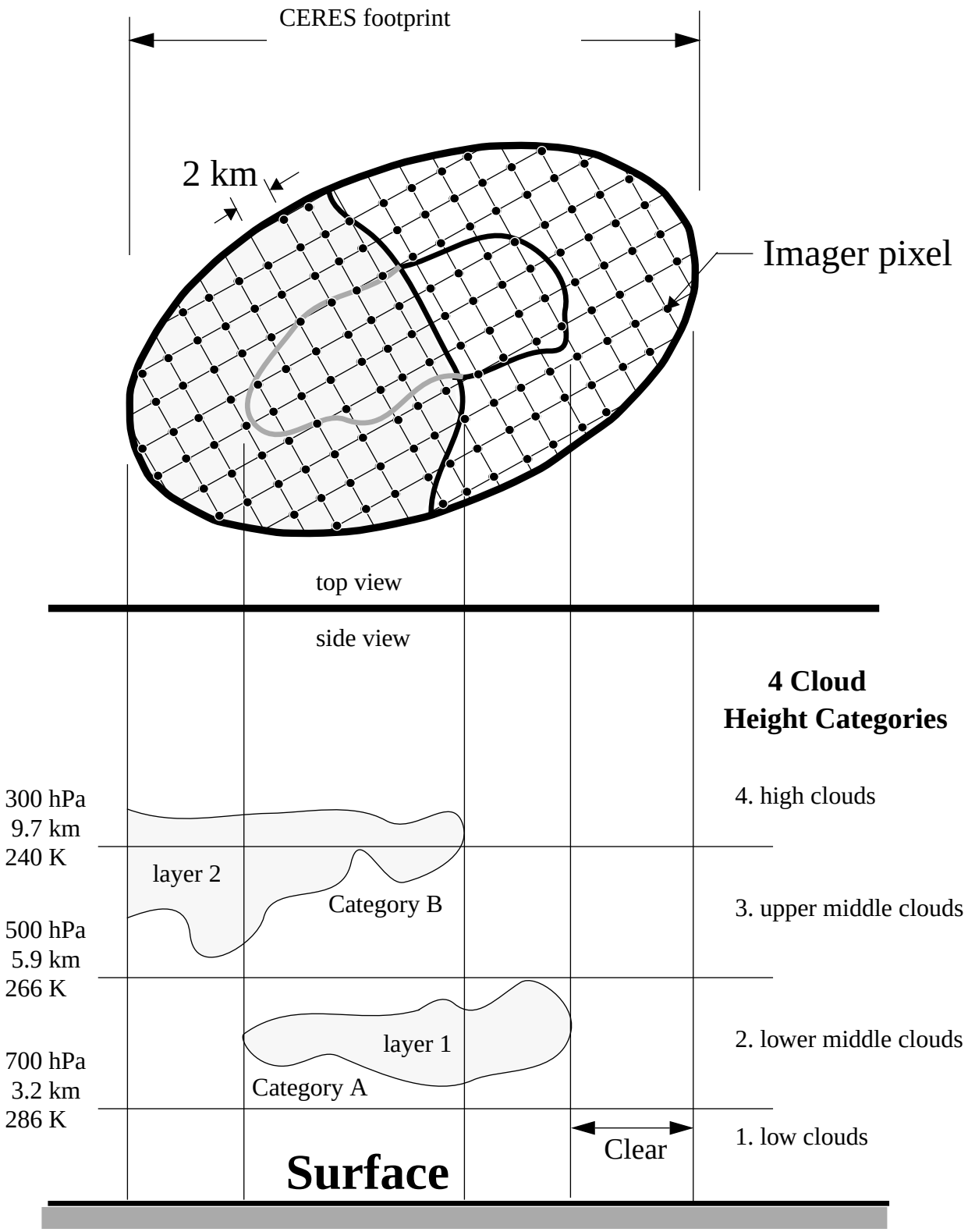

Figure 4.4-10. CERES Cloud Geometry

are only 4 possible overlap conditions within a single footprint: clear (index 1), one layer at A (index 2, 3, 4, or 5), one layer at B (index 3, 4, or 5), two layers with B over A (index 6, 7, 8, 9, 10, or 11).

We now determine the two layers and the two categories A and B from the mean clouds within the bins. The mean cloud effective pressures (#25 and #36) can range over all 4 cloud categories, but we must restrict them to categories A and B for layers 1 and 2 as discussed above. If all bins are clear, then we have no cloud categories. Let us first consider the case where all cloudy bins contain single layer clouds. We can determine the mean x and standard deviation s of the effective pressure #25 over the n bins that contain a single layer cloud. It is possible that we have not one but two single layers over the footprint. To test this, we define two layers with (x_1, s_1, n_1) and (x_2, s_2, n_2) such that $n_1 + n_2 = n$ and ${s_1}^2 + {s_2}^2$ is a minimum. If $|(x_1 - x_2)| / \sqrt{s_1^2/n_1 + s_2^2/n_2}$ is greater than 1.96, then we have two distinct layers and define categories A and B with x_1 and x_2. Otherwise the layers are not distinct and we have one layer and define category A with x.

Next, let us consider the case where all cloudy bins contain 2 cloud layers. We can determine (x, s, n) for the higher layer with #36. We can also test #36 for two distinct layers as above. If we have one layer, then we define category B with x and define category A with the mean of #25. If we have two distinct layers, then we define category A and B with x_1 and x_2 and put all lower layers (#25) into either A or B depending on which is closest.

And finally, if we have within a single footprint some bins with single layers and some bins with two layers, then we combine the first two cases. From the bins with one layer we determine (x, s, n) from #25 and also test it for two distinct layers. If #25 yields one layer and defines category A, then we determine (x, s, n) from #36 for the bins with 2 layers and determine if #25 from the single layer case and #36 give distinctly different layers. If they are different, then category B has been defined (provided A and B are not equal) and #25 from the 2 layer bins are put into the closest category. If they are not different, then clouds in the bins with 1 single layer and the top layer of the 2 layer bins are in the same layer and #25 from the two layer cases defines category B. If, however, we find that the bins with a single layer define two distinct layers, then all the cloud layers in the two layer bins are put into the closest of theses two distinct layers. Category A should be the lower cloud layer with the greater pressure. If this is not the case, then switch category A and B.

The cloud statistics over the CERES footprint as recorded as the SSF product (Table 4.4-5) are determined from the set of mean cloud parameters Table 4.4-3 for each angular bin within the footprint. For the “Full Footprint Area” we record the total number of imager pixels in the footprint. Next, we have the weighted area coverage of imager data from (4.4-17) where (i,j) range over all angular bins and x_{ij} is 1 if sampled by the imager and 0 otherwise. If the area coverage is less than 75%, then we disregard the entire footprint. In general, we determine a weighted mean by

$$\bar{x} = \frac{\sum_{\text{sampled bins}} w_{ij} x_{ij}}{\sum_{\text{sampled bins}} w_{ij}} \qquad \text{(4.4-19)}$$

and the associated weighted standard deviation as

Table 4.4-5. CERES Footprint Data on the SSF Product

Footprint Geometry

Time of CERES measurement
Satellite position (colat, long, radius)
Sun position (colat, long)
View position at TOA (colat, long)
(along-track, cross-track)
View position at Surface (colat, long)
View position at Satellite (cone, clock, scan index)
View velocity at Satellite (cone rate, clock rate)
Satellite velocity ($\dot{x}$, $\dot{y}$, $\dot{z}$)
Angles at TOA (V.Zen, S.Zen, R.Az)
Surface type coverage (8 types, altitude)
Scene types for inversion

Footprint Radiation

Radiance unfiltered (SW, LW, WN)
Flux at TOA (SW, LW, WN)
Flux at Surface (SW, LW, WN, nonWN,
NetSW, NetLW)

Full Footprint Area

Number of imager pixels in FOV
Imager percent coverage of FOV
Precipitable water
Shadowed percent coverage (TBD)
Notes on general procedure and cloud algorithms
Imager angles at TOA (mean V.Zen, mean R.Az)
Imager channel identifier (any 5 channels)
Mean imager radiances (5 channels)

Clear Footprint Area

Clear percent coverage of FOV
Sunglint percent coverage of clear area
Snow/Ice percent coverage of clear area
Smoke percent coverage of clear area
Fire percent coverage of clear area
Mean imager radiances over clear area (5 channels)
Total Aerosol in clear area (visible optical depth,
effective radius)

Cloudy Footprint Areas (for each of 2 height categories)

Cloud percent coverage of FOV
Percent overcast pixels in cloud area
Mean imager radiances over cloud area (5 channels)
Visible optical depth over cloud area (mean, std)
Log visible optical depth over cloud area (mean, std)
Infrared emissivity over cloud area (mean, std)
Liquid water path over cloud area (mean)
Ice water path over cloud area (mean)
Cloud top pressure over cloud area (mean)
Effective* pressure over cloud area (mean, std)
Effective temperature over cloud area (mean, std)
Effective height over cloud area (mean)
Cloud bottom pressure over cloud area (mean)
Water particle radius over cloud area (mean, std)
Ice particle effect. diam. over cloud area (mean, std)
Particle phase over cloud area (mean)
Vertical aspect ratio over cloud area (TBD) (mean)

Cloud Overlap Condition (for each of 4 conditions)

Overlap condition percent coverage of FOV

Abbreviations

LW - longwave channel
NetLW - net longwave
NetSW - net shortwave
PSF - Point Spread Function
R.Az - relative azimuth angle
SW - shortwave channel
S.Zen - solar zenith angle
TOA - top of atmosphere
TOT - total channel
V.Zen - viewing zenith angle
WN - window channel

* Effective as viewed from space or cloud top if optically thick and cloud center if optically thin.
# All means and Standard deviations and percent coverages are PSF weighted unless denoted otherwise.

$$S = \left[\frac{\sum_{\text{sampled bins}} w_{ij} x_{ij}^2}{\sum_{\text{sampled bins}} w_{ij}} - \bar{x}^2 \right]^{\frac{1}{2}} \quad (4.4\text{-}20)$$

where the weights w_{ij} are defined by (4.4-18) and x is the parameter of interest. From (4.4-19) we determine the weighted mean radiances for any 5 of the imager channels. We also average the imager viewing zenith and relative azimuth angles over the sampled bins which are different from the CERES angles. Recall that the imager is a cross-track scanner while the CERES can scan at any azimuth. Thus, the imager and CERES have different viewing geometries.

For the "Clear Footprint Area" we first record the coverage of clear bins from (4.4-19) where x_{ij} is 1 if clear and 0 otherwise. Next, we have the coverage of various conditions over just the clear area. For example, to determine the percent coverage of sunglint over the clear area we apply (4.4-19) where "sampled bins" is replaced by "clear bins" and x_{ij} is 1 if sunglint exist in the bin and 0 otherwise.

For the "Cloudy Footprint Areas" we record the parameters listed in Table 4.4-5 for the 2 height categories that contain the cloud layers. The actual categories can be determined by examining the mean pressures. First, we record the cloud coverage in each category from (4.4-19) where x_{ij} is the cloud fraction and is zero for bins with no clouds in the category. Since a single bin with two layers is counted in two different height categories, the sum of cloud coverage in the 2 categories plus the coverage of clear bins can exceed 100 percent. The cloud fraction in Table 4.4-3 (#2) is determined from a high resolution (250 m) cloud mask (0 or 1) and averaged over the imager FOV. The imager FOV is defined by the 11μm imager channel which at nadir is 4 km for AVHRR, 2 km for VIRS, and 1 km for MODIS. The cloud fraction is a measure of cloud brokenness and ranges in 16^{ths} from 0 to 1.

Next, we define the "percent overcast pixels" in the cloudy area. We define an overcast pixel as a pixel with a cloud fraction greater than 0.95. Since 15/16=0.94, this means that all subpixels or 16 of 16 must have a cloud mask of 1 for the imager pixel to be considered overcast. Generally, as discussed previously, the mean cloud parameters within an angular bin is the average of all pixels within the bin. The "percent overcast pixels", however, is at the pixels resolution and not the bin resolution and must be handled differently. In addition to the average of the parameters in Table 4.4-3 within a bin, we record the number of imager pixels that were averaged and the number of these pixels that were overcast. The percent of pixels within a bin that were overcast is called overcast fraction. With these definitions the "percent overcast pixels" in the cloudy area is a weighted average of the overcast fraction over just the cloudy bins.

The next 16 parameters result from determining the mean (4.4-19) and the standard deviation (4.4-20) of the cloud parameters in Table 4.4-3. The water path (#23 and #34) is sorted into two separate parameters according to particle phase (#30 and #41) so that we can form statistics on both liquid water path and ice water path. The same is true for particle radius. We also record on the SSF product the percent coverage of the 4 of 11 possible cloud overlap conditions as defined by Table 4.4-4. A more complete listing of the parameters in the SSF product are given in Section 4.0, Appendix B.

4.4.3 IMPLEMENTATION ISSUES

4.4.4 REFERENCES

Smith, G. L., 1994: Effects of time response on the point spread function of a scanning radiometer, *Appl. Opt*., **33**, 7031-7037.

Hoffman, L. H., W. L. Weaver, and J. F. Kibler, 1987: Calculation and Accuracy of ERBE Scanner Measurement Locations, *NASA Tech. Paper 2670*, 32pp.

Appendix A

Nomenclature

Acronyms

ADEOS	Advanced Earth Observing System
ADM	Angular Distribution Model
AIRS	Atmospheric Infrared Sounder (EOS-AM)
AMSU	Advanced Microwave Sounding Unit (EOS-PM)
APD	Aerosol Profile Data
APID	Application Identifier
ARESE	ARM Enhanced Shortwave Experiment
ARM	Atmospheric Radiation Measurement
ASOS	Automated Surface Observing Sites
ASTER	Advanced Spaceborne Thermal Emission and Reflection Radiometer
ASTEX	Atlantic Stratocumulus Transition Experiment
ASTR	Atmospheric Structures
ATBD	Algorithm Theoretical Basis Document
AVG	Monthly Regional, Average Radiative Fluxes and Clouds (CERES Archival Data Product)
AVHRR	Advanced Very High Resolution Radiometer
BDS	Bidirectional Scan (CERES Archival Data Product)
BRIE	Best Regional Integral Estimate
BSRN	Baseline Surface Radiation Network
BTD	Brightness Temperature Difference(s)
CCD	Charge Coupled Device
CCSDS	Consultative Committee for Space Data Systems
CEPEX	Central Equatorial Pacific Experiment
CERES	Clouds and the Earth’s Radiant Energy System
CID	Cloud Imager Data
CLAVR	Clouds from AVHRR
CLS	Constrained Least Squares
COPRS	Cloud Optical Property Retrieval System
CPR	Cloud Profiling Radar
CRH	Clear Reflectance, Temperature History (CERES Archival Data Product)
CRS	Single Satellite CERES Footprint, Radiative Fluxes and Clouds (CERES Archival Data Product)
DAAC	Distributed Active Archive Center
DAC	Digital-Analog Converter

DAO	Data Assimilation Office
DB	Database
DFD	Data Flow Diagram
DLF	Downward Longwave Flux
DMSP	Defense Meteorological Satellite Program
EADM	ERBE-Like Albedo Directional Model (CERES Input Data Product)
ECA	Earth Central Angle
ECLIPS	Experimental Cloud Lidar Pilot Study
ECMWF	European Centre for Medium-Range Weather Forecasts
EDDB	ERBE-Like Daily Data Base (CERES Archival Data Product)
EID9	ERBE-Like Internal Data Product 9 (CERES Internal Data Product)
EOS	Earth Observing System
EOSDIS	Earth Observing System Data Information System
EOS-AM	EOS Morning Crossing Mission
EOS-PM	EOS Afternoon Crossing Mission
ENSO	El Niño/Southern Oscillation
ENVISAT	Environmental Satellite
EPHANC	Ephemeris and Ancillary (CERES Input Data Product)
ERB	Earth Radiation Budget
ERBE	Earth Radiation Budget Experiment
ERBS	Earth Radiation Budget Satellite
ESA	European Space Agency
ES4	ERBE-Like S4 Data Product (CERES Archival Data Product)
ES4G	ERBE-Like S4G Data Product (CERES Archival Data Product)
ES8	ERBE-Like S8 Data Product (CERES Archival Data Product)
ES9	ERBE-Like S9 Data Product (CERES Archival Data Product)
FLOP	Floating Point Operation
FIRE	First ISCCP Regional Experiment
FIRE II IFO	First ISCCP Regional Experiment II Intensive Field Observations
FOV	Field of View
FSW	Hourly Gridded Single Satellite Fluxes and Clouds (CERES Archival Data Product)
FTM	Functional Test Model
GAC	Global Area Coverage (AVHRR data mode)
GAP	Gridded Atmospheric Product (CERES Input Data Product)
GCIP	GEWEX Continental-Phase International Project
GCM	General Circulation Model
GEBA	Global Energy Balance Archive
GEO	ISSCP Radiances (CERES Input Data Product)

GEWEX	Global Energy and Water Cycle Experiment
GLAS	Geoscience Laser Altimetry System
GMS	Geostationary Meteorological Satellite
GOES	Geostationary Operational Environmental Satellite
HBTM	Hybrid Bispectral Threshold Method
HIRS	High-Resolution Infrared Radiation Sounder
HIS	High-Resolution Interferometer Sounder
ICM	Internal Calibration Module
ICRCCM	Intercomparison of Radiation Codes in Climate Models
ID	Identification
IEEE	Institute of Electrical and Electronics Engineers
IES	Instrument Earth Scans (CERES Internal Data Product)
IFO	Intensive Field Observation
INSAT	Indian Satellite
IOP	Intensive Observing Period
IR	Infrared
IRIS	Infrared Interferometer Spectrometer
ISCCP	International Satellite Cloud Climatology Project
ISS	Integrated Sounding System
IWP	Ice Water Path
LAC	Local Area Coverage (AVHRR data mode)
LaRC	Langley Research Center
LBC	Laser Beam Ceilometer
LBTM	Layer Bispectral Threshold Method
Lidar	Light Detection and Ranging
LITE	Lidar In-Space Technology Experiment
Lowtran 7	Low-Resolution Transmittance (Radiative Transfer Code)
LW	Longwave
LWP	Liquid Water Path
MAM	Mirror Attenuator Mosaic
MC	Mostly Cloudy
MCR	Microwave Cloud Radiometer
METEOSAT	Meteorological Operational Satellite (European)
METSAT	Meteorological Satellite
MFLOP	Million FLOP
MIMR	Multifrequency Imaging Microwave Radiometer
MISR	Multiangle Imaging Spectroradiometer
MLE	Maximum Likelihood Estimate

MOA	Meteorology Ozone and Aerosol
MODIS	Moderate-Resolution Imaging Spectroradiometer
MSMR	Multispectral, multiresolution
MTSA	Monthly Time and Space Averaging
MWH	Microwave Humidity
MWP	Microwave Water Path
NASA	National Aeronautics and Space Administration
NCAR	National Center for Atmospheric Research
NCEP	National Centers for Environmental Prediction
NESDIS	National Environmental Satellite, Data, and Information Service
NIR	Near Infrared
NMC	National Meteorological Center
NOAA	National Oceanic and Atmospheric Administration
NWP	Numerical Weather Prediction
OLR	Outgoing Longwave Radiation
OPD	Ozone Profile Data (CERES Input Data Product)
OV	Overcast
PC	Partly Cloudy
POLDER	Polarization of Directionality of Earth's Reflectances
PRT	Platinum Resistance Thermometer
PSF	Point Spread Function
PW	Precipitable Water
RAPS	Rotating Azimuth Plane Scan
RPM	Radiance Pairs Method
RTM	Radiometer Test Model
SAB	Sorting by Angular Bins
SAGE	Stratospheric Aerosol and Gas Experiment
SARB	Surface and Atmospheric Radiation Budget Working Group
SDCD	Solar Distance Correction and Declination
SFC	Hourly Gridded Single Satellite TOA and Surface Fluxes (CERES Archival Data Product)
SHEBA	Surface Heat Budget in the Arctic
SPECTRE	Spectral Radiance Experiment
SRB	Surface Radiation Budget
SRBAVG	Surface Radiation Budget Average (CERES Archival Data Product)
SSF	Single Satellite CERES Footprint TOA and Surface Fluxes, Clouds
SSMI	Special Sensor Microwave Imager
SST	Sea Surface Temperature

SURFMAP	Surface Properties and Maps (CERES Input Product)
SW	Shortwave
SWICS	Shortwave Internal Calibration Source
SYN	Synoptic Radiative Fluxes and Clouds (CERES Archival Data Product)
SZA	Solar Zenith Angle
THIR	Temperature/Humidity Infrared Radiometer (Nimbus)
TIROS	Television Infrared Observation Satellite
TISA	Time Interpolation and Spatial Averaging Working Group
TMI	TRMM Microwave Imager
TOA	Top of the Atmosphere
TOGA	Tropical Ocean Global Atmosphere
TOMS	Total Ozone Mapping Spectrometer
TOVS	TIROS Operational Vertical Sounder
TRMM	Tropical Rainfall Measuring Mission
TSA	Time-Space Averaging
UAV	Unmanned Aerospace Vehicle
UT	Universal Time
UTC	Universal Time Code
VAS	VISSR Atmospheric Sounder (GOES)
VIRS	Visible Infrared Scanner
VISSR	Visible and Infrared Spin Scan Radiometer
WCRP	World Climate Research Program
WG	Working Group
Win	Window
WN	Window
WMO	World Meteorological Organization
ZAVG	Monthly Zonal and Global Average Radiative Fluxes and Clouds (CERES Archival Data Product)

Symbols

A	atmospheric absorptance
$B_\lambda(T)$	Planck function
C	cloud fractional area coverage
CF_2Cl_2	dichlorofluorocarbon
$CFCl_3$	trichlorofluorocarbon
CH_4	methane
CO_2	carbon dioxide
D	total number of days in the month
D_e	cloud particle equivalent diameter (for ice clouds)

E_o	solar constant or solar irradiance
F	flux
f	fraction
G_a	atmospheric greenhouse effect
g	cloud asymmetry parameter
H_2O	water vapor
I	radiance
i	scene type
m_i	imaginary refractive index
$\hat{N}$	angular momentum vector
N_2O	nitrous oxide
O_3	ozone
P	point spread function
p	pressure
Q_a	absorption efficiency
Q_e	extinction efficiency
Q_s	scattering efficiency
R	anisotropic reflectance factor
r_E	radius of the Earth
r_e	effective cloud droplet radius (for water clouds)
r_h	column-averaged relative humidity
S_o	summed solar incident SW flux
S_o'	integrated solar incident SW flux
T	temperature
T_B	blackbody temperature
t	time or transmittance
W_{liq}	liquid water path
w	precipitable water
$\hat{x}_o$	satellite position at t_o
x, y, z	satellite position vector components
$\dot{x}, \dot{y}, \dot{z}$	satellite velocity vector components
z	altitude
z_{top}	altitude at top of atmosphere
α	albedo or cone angle
β	cross-scan angle
γ	Earth central angle
γ_{at}	along-track angle
γ_{ct}	cross-track angle

δ	along-scan angle
ε	emittance
Θ	colatitude of satellite
θ	viewing zenith angle
θ_o	solar zenith angle
λ	wavelength
μ	viewing zenith angle cosine
μ_o	solar zenith angle cosine
ν	wave number
ρ	bidirectional reflectance
τ	optical depth
$\tau_{aer}(p)$	spectral optical depth profiles of aerosols
$H_2O\lambda^{(p)}$	spectral optical depth profiles of water vapor
$\tau_{O_3}(p)$	spectral optical depth profiles of ozone
Φ	longitude of satellite
ϕ	azimuth angle
ω_o	single-scattering albedo

Subscripts:

c	cloud
cb	cloud base
ce	cloud effective
cld	cloud
cs	clear sky
ct	cloud top
ice	ice water
lc	lower cloud
liq	liquid water
s	surface
uc	upper cloud
λ	spectral wavelength

Units

AU	astronomical unit
cm	centimeter
cm-sec^{-1}	centimeter per second
count	count
day	day, Julian date
deg	degree

deg-sec^{-1}	degree per second
DU	Dobson unit
erg-sec^{-1}	erg per second
fraction	fraction (range of 0–1)
g	gram
g-cm^{-2}	gram per square centimeter
g-g^{-1}	gram per gram
g-m^{-2}	gram per square meter
h	hour
hPa	hectopascal
K	Kelvin
kg	kilogram
kg-m^{-2}	kilogram per square meter
km	kilometer
km-sec^{-1}	kilometer per second
m	meter
mm	millimeter
μm	micrometer, micron
N/A	not applicable, none, unitless, dimensionless
ohm-cm^{-1}	ohm per centimeter
percent	percent (range of 0–100)
rad	radian
rad-sec^{-1}	radian per second
sec	second
sr^{-1}	per steradian
W	watt
W-m^{-2}	watt per square meter
W-m^{-2}sr^{-1}	watt per square meter per steradian
W-m^{-2}sr^{-1}μm^{-1}	watt per square meter per steradian per micrometer